

From Knock-Out Phenotype to Three-Dimensional Structure of a Promising Antibiotic Target from *Streptococcus pneumoniae*

Con Dogovski^{1,2}, Michael A. Gorman³, Natalia E. Ketaren², Judy Praszkiar⁴, Leanne M. Zammit¹, Haydyn D. Mertens⁵, Gary Bryant⁶, Ji Yang⁴, Michael D. W. Griffin², F. Grant Pearce⁷, Juliet A. Gerrard^{7,8}, Geoffrey B. Jameson⁹, Michael W. Parker^{2,3}, Roy M. Robins-Browne⁴, Matthew A. Perugini^{1,2}

1 Department of Biochemistry, La Trobe Institute for Molecular Science, La Trobe University, Melbourne, Victoria, Australia, **2** Department of Biochemistry and Molecular Biology, Bio21 Molecular Science and Biotechnology Institute, University of Melbourne, Victoria, Australia, **3** St Vincent's Institute of Medical Research, Fitzroy, Victoria, Australia, **4** Department of Microbiology & Immunology, University of Melbourne, Victoria, Australia, **5** Australian Synchrotron, Clayton, Victoria, Australia, **6** School of Applied Sciences, RMIT University, Melbourne, Victoria, Australia, **7** Biomolecular Interaction Centre and School of Biological Sciences, University of Canterbury, Christchurch, New Zealand, **8** Callaghan Innovation, Lower Hutt, New Zealand, **9** Centre for Structural Biology, Institute of Fundamental Sciences, Massey University, Palmerston North, New Zealand

Abstract

Given the rise in drug-resistant *Streptococcus pneumoniae*, there is an urgent need to discover new antimicrobials targeting this pathogen and an equally urgent need to characterize new drug targets. A promising antibiotic target is dihydrodipicolinate synthase (DHDPS), which catalyzes the rate-limiting step in lysine biosynthesis. In this study, we firstly show by gene knock out studies that *S. pneumoniae* (*sp*) lacking the DHDPS gene is unable to grow unless supplemented with lysine-rich media. We subsequently set out to characterize the structure, function and stability of the enzyme drug target. Our studies show that *sp*-DHDPS is folded and active with a $k_{cat} = 22 \text{ s}^{-1}$, $K_M^{PYR} = 2.55 \pm 0.05 \text{ mM}$ and $K_M^{ASA} = 0.044 \pm 0.003 \text{ mM}$. Thermal denaturation experiments demonstrate *sp*-DHDPS exhibits an apparent melting temperature (T_M^{app}) of 72 °C, which is significantly greater than *Escherichia coli* DHDPS (*Ec*-DHDPS) ($T_M^{app} = 59 \text{ °C}$). Sedimentation studies show that *sp*-DHDPS exists in a dimer-tetramer equilibrium with a $K_D^{4 \rightarrow 2} = 1.7 \text{ nM}$, which is considerably tighter than its *E. coli* ortholog ($K_D^{4 \rightarrow 2} = 76 \text{ nM}$). To further characterize the structure of the enzyme and probe its enhanced stability, we solved the high resolution (1.9 Å) crystal structure of *sp*-DHDPS (PDB ID 3VFL). The enzyme is tetrameric in the crystal state, consistent with biophysical measurements in solution. Although the *sp*-DHDPS and *Ec*-DHDPS active sites are almost identical, the tetramerization interface of the *s. pneumoniae* enzyme is significantly different in composition and has greater buried surface area (800 Å²) compared to its *E. coli* counterpart (500 Å²). This larger interface area is consistent with our solution studies demonstrating that *sp*-DHDPS is considerably more thermally and thermodynamically stable than *Ec*-DHDPS. Our study describe for the first time the knock-out phenotype, solution properties, stability and crystal structure of DHDPS from *S. pneumoniae*, a promising antimicrobial target.

Citation: Dogovski C, Gorman MA, Ketaren NE, Praszkiar J, Zammit LM, et al. (2013) From Knock-Out Phenotype to Three-Dimensional Structure of a Promising Antibiotic Target from *Streptococcus pneumoniae*. PLoS ONE 8(12): e83419. doi:10.1371/journal.pone.0083419

Editor: Paul Taylor, University of Edinburgh, United Kingdom

Received: September 12, 2013; **Accepted:** November 13, 2013; **Published:** December 13, 2013

Copyright: © 2013 Dogovski et al. This is an open-access article distributed under the terms of the Creative Commons Attribution License, which permits unrestricted use, distribution, and reproduction in any medium, provided the original author and source are credited.

Funding: Funding provided by (1) Australian Research Council Future Fellowship FT0991245, (2) National Health & Medical Research Council (NHMRC) Project Grant 6286811 (3) NHMRC Fellowship APP1021645. The funders had no role in study design, data collection and analysis, decision to publish, or preparation of the manuscript.

Competing interests: The authors have declared that no competing interests exist.

* E-mail: M.Perugini@latrobe.edu.au

☉ These authors contributed equally to this work.

Introduction

Streptococcus pneumoniae is a Gram-positive bacterium and human commensal inhabiting the upper respiratory tract [1]. The organism often causes pneumonia in children, the elderly and immunocompromized, and if left untreated can result in death [2]. Pneumonia accounts for the death of approximately

1 million children per annum under the age of 5, making this disease the leading cause of childhood mortality worldwide [2,3]. In recent years *S. pneumoniae* has received considerable attention due to the emergence of multi-drug resistant strains, commonly referred to as drug-resistant *Streptococcus pneumoniae* (DRSP) [3,4]. Standard antimicrobial treatment options, such as the β-lactam and macrolide antibiotics, are

Table 1. Sequences of primers employed in the *S. pneumoniae* *dapA* knock out experiments.

Primer	Sequence
pVA838.F	CACAAGTGATTGTGATTGTTG
pVA838.R	GCGCTTAGTGGGAATTTGTAC
dapERM.F	GTACAAATCCCACTAAGCGCGTCGTAGATGGCGACTACGAAGC
dapERM.R	CAACAATCACAATCACTTTGTGCAATCAAGGCTGGAATAGCATC
dap.F	CGAAGAGATGAAGATGACCAAGG
dap.R	GAATCAACAACCTCTTTTGAAGATGC
OCD52	CACGTGATTGTCATGCGGAA
OCD53	ATCGGTGTTGAGCGTTTCGAA

doi: 10.1371/journal.pone.0083419.t001

Construction of the *S. pneumoniae* 447A Δ *dapA* mutant strain

Overlapping extension PCR [40] was used to generate a DNA fragment carrying the erythromycin resistance (Em^R) gene flanked by regions up and downstream of *S. pneumoniae* 447A *dapA*. Briefly, primer pairs *dap.F/dapERM.R* and *dapERM.F/dap.R* (Table 1) were used to amplify DNA flanking the region to be deleted from the chromosome of *S. pneumoniae* 447A, and primers *pVA838.F/pVA838.R* (Table 1) were used to amplify the Em^R gene from plasmid *pVA838* [41]. The products of these three PCR reactions (100 ng each) served as template in overlapping extension PCR using primers *dap.F/dap.R* (Table 1) to generate a linear construct, which was cloned into *pGEM-T Easy* (Promega, Madison, WI), introduced into *E. coli* K-12 TOP10 cells and confirmed by sequencing. The *pGEM-T Easy* construct was used as a template in a PCR with primers *dap.F/dap.R*, to amplify the linear allelic replacement DNA fragment, which was introduced into *S. pneumoniae* 447A by transformation. The Δ *dapA* mutation was confirmed by PCR using primer pairs in which one primer flanked the targeted region and the other primed within the Em^R gene (OCD52/*dapERM.R* and OCD53/*dapERM.F*). The PCR products were sequenced using primers OCD52 and OCD53 (Table 1).

Transformation of *S. pneumoniae* 447A

Bacteria were grown in c-CAT medium (1% w/v Casamino acids, 0.5% w/v Tryptone, 0.5% w/v NaCl, 1% w/v Yeast Extract, 16 mM K_2HPO_4 , 0.2 % w/v glucose, 15 μ g ml⁻¹ glutamine) at 37°C to OD₆₀₀ of 0.25-0.30. Cells were diluted 1/10 in 10 ml CTM medium (c-CAT containing 0.2% BSA and 1 mM $CaCl_2$), grown at 37°C to OD₆₀₀ of 0.10, collected by centrifugation and resuspended in 1 ml of 15% v/v glycerol prepared in CTM adjusted to pH 7.8. 100 μ l aliquots of cell suspension were stored at -80°C until required. For transformation, 100 μ l of cells were thawed on ice, 1 ml of CTM-pH 7.8 and 100 ng of synthetic competence-stimulating peptide 1 (CSP-1) [42] were added and cells incubated at 37°C for 13 min. DNA was added and cells were incubated at 32°C for 35 min then incubation continued for 3 hours at 37°C. Transformation mixture was plated out on HBA containing 0.1 μ g ml⁻¹ erythromycin and incubated overnight at 37°C in an atmosphere of 5% CO₂.

Expression and purification of Sp-DHDPS

Recombinant *Sp*-DHDPS was expressed, purified and assessed by SDS-PAGE and mass spectrometry to be >95% homogeneous as described previously [43].

Coupled kinetics assay

Kinetic studies were conducted using the coupled-assay method as previously described [16,36,44,45]. Data were collected on a Cary UV-Vis spectrophotometer (Varian) connected to a Peltier cell to maintain a constant temperature of 30°C. Assays were performed in 1.5 ml semi-micro acrylic cuvettes with a path length of 10 mm. (S)-ASA was synthesized according to the methods of Roberts et al. [46]. A standard assay contained 20 nM of DHDPS, 250 mM HEPES pH 8.0, 0.2 mM NADPH, varied concentrations of pyruvate and (S)-ASA, 75 μ g ml⁻¹ of DHDPR (purified from *E. coli*) in a final volume of 0.8 ml. Cuvettes were pre-incubated at 30°C for 8 min before the reaction was initiated *via* the addition of (S)-ASA. Rates were determined from the initial linear portion of the data collected. The background degradation of NADPH was factored into rate calculations and each data point was measured in triplicate within a <10% error margin.

Circular dichroism (CD) spectroscopy

CD spectroscopy experiments were performed on an Aviv Model 420SF CD spectrometer using a 1.0 nm bandwidth. CD spectra of *Sp*-DHDPS were recorded at a protein concentration of 4.5 μ M solubilized in 20 mM Tris-HCl pH 8.0 and 150 mM NaCl. Wavelength scans spanning 195-240 nm were measured using a step size of 0.5 nm with a 2 sec averaging time in a 1 mm stoppered quartz cuvette as reported previously [16,36,47]. The resulting spectra were analyzed using the CONTINLL algorithm and SP43 database employing the CDPRO software package [48,49]. Thermal denaturation experiments were monitored at 222 nm over a temperature range of 4–90°C collecting data at 1°C intervals with a 5 s averaging time. Given that DHDPS requires chaperones to fold [50], the denaturation of DHDPS enzymes is irreversible *in vitro*, and therefore the apparent melting temperature (T_M^{app}), or midpoint of the transition between folded to unfolded state, was determined empirically from the ordinate maximum of the first derivative of the thermal denaturation profile [36].

Analytical ultracentrifugation

Analytical ultracentrifugation (AUC) studies were conducted in a XL-I analytical ultracentrifuge (Beckman Coulter) using 12 mm double sector cells with quartz windows loaded into either an An-60 Ti 4-hole rotor or An-50 Ti 8-hole rotor at a temperature of 20°C. *Sp*-DHDPS samples for all centrifugation runs were solubilized in 20 mM Tris-HCl pH 8.0 and 150 mM NaCl. For sedimentation velocity experiments, 380 μ L of sample and 400 μ L of reference (20 mM Tris-HCl pH 8.0 and 150 mM NaCl) were employed and absorbance *versus* radial profiles were generated at 40,000 rpm in continuous mode using a step size of 0.003 cm and a radial range of 5.8–7.3 cm without averaging. Data were collected at wavelengths of 210 nm (296–740 nM *Sp*-DHDPS) or 230 nm (4.5 μ M *Sp*-DHDPS).

The absorbance versus radii profiles at different time points were fitted to single discrete species or a continuous size-distribution model using the program SEDFIT [51,52] (available from www.analyticalultracentrifugation.com). The program SEDNTRP [53,54] was used to determine the partial specific volume of Sp-DHDPS (0.7475 ml g^{-1}), buffer density (1.005 g ml^{-1}) and buffer viscosity (1.021 cp) at 20°C . For sedimentation equilibrium experiments, $120 \mu\text{L}$ of reference solution and $100 \mu\text{L}$ of sample at three initial protein concentrations (i.e. 296 nM , 355 nM and 740 nM) were centrifuged at rotor speeds of $10,000 \text{ rpm}$ and $18,000 \text{ rpm}$. Initial absorbance versus radial profiles were measured at 210 nm between 6.8 and 7.2 cm in step mode using a 0.001 cm step size and 3 averages until sedimentation equilibrium was attained ($t \sim 24 \text{ hours}$). At sedimentation equilibrium, detailed absorbance versus radius scans were taken using a step size of 0.001 cm over a radial range of 6.8 to 7.2 cm with 15 replicates. The resulting absorbance versus radial position profiles at multiple sample concentrations and rotor speeds were globally fitted to a single discrete species model or various self-associating models (including monomer-dimer, monomer-trimer, dimer-tetramer, trimer-hexamer and monomer-dimer-tetramer models) using the program SEDPHAT [55] (available from www.analyticalultracentrifugation.com).

Dynamic light scattering

Dynamic light scattering measurements were made on an ALV 5022F DLS (ALV, Germany). Protein samples were analyzed at a final concentration of $59 \mu\text{M}$. Measurements were taken over a 30 s time period with 10 replicates at 20°C . The samples were illuminated with a HeNe laser (633 nm) and experiments were conducted at a scattering angle of 90 degrees. The in-built ALV analysis software was used to determine average radii.

Crystallization

Crystallization of Sp-DHDPS was performed as previously described [40]. Briefly, crystals were obtained by employing the hanging-drop vapor-diffusion method. $1 \mu\text{l}$ protein solution (10 mg ml^{-1}) and $1 \mu\text{l}$ precipitant solution were equilibrated against 1 ml reservoir solution [0.2 M ammonium chloride, 20% (w/v) PEG 6000, 0.1 M MES pH 6.0] in 24-well Linbro plates at 20°C . Crystals were soaked briefly in cryoprotectant composed of 0.2 M ammonium chloride, 20% (w/v) PEG 6000, 0.1 M MES pH 6.0 and 20% (w/v) glycerol and were then flash-frozen using liquid nitrogen.

Structure determination

X-ray diffraction experiments were carried out at the Australian Synchrotron, Victoria, Australia on the MX1 beamline using Blu-Ice [56]. A 1.9 \AA resolution data set was integrated and merged with HKL2000 [57] and scaled with SCALA [58]. The crystals were initially assigned to the tetragonal crystal system, space group $P4_2,2_1,2$ with unit cell dimensions $a = b = 105.5 \text{ \AA}$ and $c = 62.4 \text{ \AA}$, and an overall R_{merge} of 6% . Molecular replacement was carried out using the program PHASER [59] with the structure of dihydrodipicolinate synthase from *B. anthracis* (PDB ID: 1XL9) [22] as the search

model. One molecule was located in the asymmetric unit. The structure was refined using the program PHENIX [60] with rigid body refinement, simulated annealing and atomic displacement parameters (ADP) refinement. Iterative model building was carried out using the program COOT [61] followed by ADP refinement. Even though the $2F_o - F_c$ electron density map was clear, there were spurious streaks in the $F_o - F_c$ difference maps and refinement stalled with a R_{work} of 24% and a R_{free} of 32% . Examination of the cumulative intensity plot from SCALA suggested that the data were affected by crystal twinning. The data were inspected further by running the program phenix.xtriage. Since there are no twin laws possible in the above crystal symmetry, over-merging of pseudo-symmetric or twinned data may have been present. The diffraction data were re-integrated in space group P1 using XDS [62] and further analyzed with phenix.xtriage. The presence of seven pseudo-merohedral twin operators were found, two 4-fold and five 2-fold. The twin law giving the lowest R_{obs} was $-h, l, k$ superimposing on h, k, l . The data were scaled in space group P2 (cell dimensions $a = 64.4 \text{ \AA}$, $b = 105.3 \text{ \AA}$, $c = 105.5 \text{ \AA}$, $\beta = 90.0^\circ$ degrees) and refined as above with the inclusion of the above two-fold twin law and four crystallographically-independent subunits (residues 2-299 and 2-297) in the asymmetric unit leading to values for R_{work} of 19.7% and R_{free} of 22.9% (this model has been deposited with PDB ID: 3H5D). However, inspection of the diffraction data and the structural model provided clear evidence for 2_1 screw axes perpendicular to the monoclinic unique b axis. The twinning axis is parallel to the crystallographic two-fold axis (which is a pseudo- 4_2 or 2_1 screw axis with significant intensity violations), leading to reflections $-k, h, l$ being overlapped with h, k, l and to the observed pseudo-tetragonal $4/mmm$ Laue symmetry. The final model, now in space group $P2_2,2_1$, was solved by molecular replacement using MOLREP [63] with the model PDB ID: 3HIJ [36] together with amplitude-based twin refinement with NCS restraints using REFMAC5 [64]. The final model ($R_{\text{work}} = 16.5\%$ and $R_{\text{free}} = 21.2\%$) comprises of two monomers (residues A2 – A299 and B2 – B297, and A302 – A311 and B302 – B311), 235 water molecules, 4 potassium ions, 4 glycerol molecules and 2 MeS ions. The pseudo-tetragonal symmetry leads to two possible choices of asymmetric unit, one comprising a pair of subunits forming the ‘weak’ dimer interface, the other comprising a pair of subunits forming the ‘tight’ interface – the usual asymmetric unit seen in other tetrameric DHDPS structures. Both were tested, the latter being confirmed as correct. The crystallographic two-fold axis generates the tetramer. Residues 300-301 of chain A and residues 298-301 of chain B were not observed in electron density maps, and as a result of crystal packing, it is not unequivocally clear whether the C-terminal residues 302-311, which were very clearly defined in electron density maps once the twinning and space group problems were solved, indulge in domain swapping to a neighboring tetramer or remain with their own tetramer. However, electrospray ionization mass spectrometry analysis of dissolved crystals of recombinant Sp-DHDPS indicates that the entire protein (residues 1-311) is intact. A summary of the crystallographic data collection and refinement statistics is provided in Table 2.

Table 2. Data collection and refinement statistics for the X-ray structure of Sp-DHDPS (PDB ID: 3VFL).

Temperature (K)	100
Space group	P22₁2₁
Cell dimensions A (a, b, c)	62.4, 105.3, 105.5
Resolution (Å)	74.6 -1.9
No. of observations	757223
No. of unique observations	51243
Completeness (%)	99.6 (97.7) ¹
I/σ ₁	35.7 (4.7)
R _{sym} (%) ²	6.3 (56.2)
Twin operator	-h, l, k
Twin fraction	0.46
Wilson B factor Å ²	22.6
REFINEMENT STATISTICS	
Non-hydrogen atoms	
Protein	4725
Water	235
Ligands	52
R _{work} (%) ³	16.5
R _{free} (%) ⁴	21.2
RMSD values from ideal value	
Bond lengths (Å)	0.02
Bond angles (°)	2.4
Ramachandran plot	
Most favored and allowed region (%)	99.3
B factors (Å²)	
Average main chain	27.8
Average side chain	29.6
Average water molecule	29.9

¹ Values in parentheses represent the highest resolution shell (2.1–1.9).

² $R_{\text{sym}} = \sum |I - \langle I \rangle| / \sum I$.

³ $R_{\text{work}} = \sum ||F_{\text{o}}| - |F_{\text{c}}|| / \sum |F_{\text{o}}|$.

⁴ R_{free} is based on 5% of the total reflections excluded from refinement.

doi: 10.1371/journal.pone.0083419.t002

Coordinates

Coordinates and structure factors for the final model are accessible *via* the Protein Data Bank (PDB ID: 3VFL).

Results

S. pneumoniae 447A Δ dapA mutant requires (S)-lysine for growth

To validate DHDPS as a promising drug target in *Streptococcus pneumoniae*, the gene encoding this enzyme (i.e. *dapA*) was deleted from strain 447A. The Δ dapA mutant was generated by homologous recombination as described in the Materials and Methods. Cultivation of the Δ dapA and wild-type strains on nutrient-rich media, such as HBA, showed that their size and morphology were indistinguishable (data not shown). To determine whether the Δ dapA mutant required (S)-lysine for growth, wild-type and mutant strains were grown in Chemically Defined Medium CDM⁺ and CDM⁻ (where + and - indicates the presence and absence of 200 $\mu\text{g ml}^{-1}$ (S)-lysine,

respectively) at 37°C in an atmosphere of 5% CO₂. Analysis of growth rates of wild-type and Δ dapA mutant strains showed that the rate of growth of the mutant in CDM⁺ was not significantly different to that of the wild-type strain (Figure 2). However, the Δ dapA mutant was unable to grow in CDM⁻ whereas the wild-type strain reached comparable cell density in CDM⁺ and CDM⁻ (Figure 2). This demonstrates that the *dapA* gene, encoding DHDPS, is essential for the growth of *S. pneumoniae* in the absence of lysine.

Secondary structure and stability of Sp-DHDPS

Sp-DHDPS was expressed and purified to >95% homogeneity as described previously [43]. The enzyme was subjected to circular dichroism (CD) spectroscopy in aqueous solution to assess the secondary structure of the recombinant product. The CD spectrum (Figure 3A) shows a broad minimum spanning 208 nm to 222 nm, suggesting Sp-DHDPS adopts a mixed α/β secondary structure in solution [16,36,47]. This assertion was confirmed by fitting the CD spectrum of Sp-DHDPS to the CONTINLL algorithm and SP43 database using the CDPRO software suite [48,49]. The nonlinear best-fit demonstrates a significant proportion of α -helix and β -strand (Table 3). The calculated secondary structure composition of Sp-DHDPS is comparable to that of DHDPS enzymes from other bacteria, including *E. coli* (Table 3). Next we assessed the stability of recombinant Sp-DHDPS in solution by conducting thermal denaturation experiments monitored by CD at 222 nm (Figure 3B). The resulting thermal denaturation profile reveals that the enzyme unfolds *via* a single transition with an apparent melting temperature ($T_{\text{M}}^{\text{app}}$) of 72°C (Figure 3B and Table 4). Recombinant DHDPS from *E. coli* (*Ec*-DHDPS) also unfolds *via* a single transition, but with a significantly lower $T_{\text{M}}^{\text{app}}$ of 59°C (Figure 3B and Table 4). These data therefore indicate that Sp-DHDPS is markedly more stable in solution than *Ec*-DHDPS. We were thus interested in unraveling the molecular mechanism for this enhanced thermostability by assessing the quaternary structure of Sp-DHDPS in solution.

Quaternary structure of Sp-DHDPS in aqueous solution

To gain further insights into the solution stability of Sp-DHDPS, sedimentation velocity studies were conducted in the analytical ultracentrifuge. Absorbance *versus* radial data profiles at different time points were fitted to a continuous size-distribution, $c(s)$, model [51,52,65,66]. The resulting $c(s)$ distribution for Sp-DHDPS at an initial concentration of 4.5 μM is shown in Figure 4A. The $c(s)$ distribution reveals a single peak with a $s_{20,w}$ value of 7.2 S that is consistent with a tetrameric species (Table 4) [34,36]. The corresponding $c(M)$ distribution (Figure 4B) confirmed this assertion and shows a single peak with a molar mass of 133 kDa, which closely matches the theoretical mass of the Sp-DHDPS tetramer (135 kDa). Sedimentation studies at a 6-fold lower protein concentration (i.e. 740 nM) were conducted and the resulting $c(s)$ nonlinear least-squares fit also reveals the presence of a single peak (Figure 4B) with a $s_{20,w}$ value of 7.0 S, consistent with the enzyme existing primarily as a tetramer [26,27,34,36]. These sedimentation velocity analyses suggest that Sp-

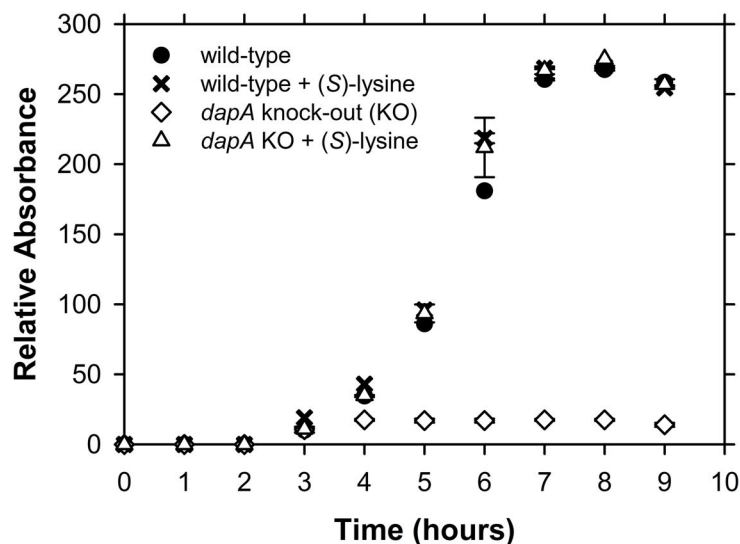


Figure 2. Growth phenotype of the *dapA* knockout strain of *S. pneumoniae*. Growth of wt *S. pneumoniae* 447A (control) and the Δ *dapA* mutant strain in the presence and absence of 20 mM (S)-lysine. Growth was assessed by monitoring the optical density (Relative Absorbance) of duplicate cultures on an hourly basis as described in the Materials and Methods.

doi: 10.1371/journal.pone.0083419.g002

DHDPS exists as a very stable tetramer in solution. Sedimentation equilibrium experiments were subsequently performed in the analytical ultracentrifuge to examine the strength of subunit interactions and the resulting data at multiple protein concentrations fitted to various equilibrium schemes. Not surprisingly, the optimal global nonlinear least-squares fit was obtained for a dimer-tetramer equilibrium model (Figure 5, solid lines) with a tetramer-dimer dissociation constant (K_D^{42}) of 1.7 nM. Interestingly, the calculated K_D^{42} for *Sp*-DHDPS is considerably tighter than that obtained for the previously characterized *Ec*-DHDPS tetramer (Table 4) [34]. We next set out to determine the average hydrodynamic radius of the *Sp*-DHDPS tetramer in solution using dynamic light scattering.

The hydrodynamic radius of the *Sp*-DHDPS tetramer

The quaternary structure and hydrodynamic radius of *Sp*-DHDPS were studied by dynamic light scattering (DLS) experiments at an enzyme concentration of 59 μ M [3.5×10^4 -fold above the K_D^{4-2} of *Sp*-DHDPS (Table 4)]. The resulting data were analyzed by the method of cumulants (second-order) and were found to be reproducible between runs and independent of the choice of fit range. Figure 4D shows a regularized distribution fit employing the in-built software (ALV). Analysis of data resulted in a range of hydrodynamic radii that centered on an average value of 4.5 ± 0.2 nm. The average hydrodynamic radius was consistent between runs and was not affected by the choice of fit parameters (correlation function limits or radius limits). By comparison, the Stokes radius of the tetramer calculated from sedimentation velocity studies is 4.3 nm, which is in excellent agreement with the DLS experiment.

Enzyme kinetic properties of *Sp*-DHDPS

To characterize the catalytic properties of the *Sp*-DHDPS tetramer, we employed the DHDPS-DHDPR coupled assay [45] at an enzyme concentration of 20 nM, which is ~ 12 -fold greater than the K_D^{4-2} (Table 4). Initial rates were measured with fixed pyruvate concentrations of 0.5 mM, 1.0 mM, 2.0 mM, 4.0 mM, 8.0 mM and 16.0 mM and varying ASA concentrations (0–0.48 mM). The resulting data were expressed initially as Lineweaver-Burk plots (Figure 6A), which displayed a characteristic series of parallel lines indicating that *Sp*-DHDPS follows a Ping-Pong kinetic mechanism [67]. This mechanism has been demonstrated for DHDPS orthologs from other bacterial species, including *Ec*-DHDPS [45,68,69]. The data were subsequently plotted to produce Michaelis-Menten profiles (Figure 6B) and fitted to bi-substrate kinetic models (with and without substrate inhibition), namely the ternary complex and Ping-Pong mechanism employing ENZFITTER software (Biosoft). The global nonlinear regression analysis yielded a best-fit to a Ping-Pong model with no substrate inhibition (Figure 6B, solid lines) that resulted in a $R^2 = 0.98$ and the kinetic parameters reported in Table 5. The K_M of *Sp*-DHDPS for (S)-ASA is similar that for the *E. coli* enzyme (Table 5). However, the K_M for pyruvate is 10-fold higher than that for *Ec*-DHDPS, and the catalytic turnover (k_{cat}) is 6-fold lower for *Sp*-DHDPS compared to the *E. coli* ortholog (Table 5).

Crystal structure of *Sp*-DHDPS

In order to gain further insight into the stability and kinetic behavior at the atomic level, we next sought to determine the crystal structure of *Sp*-DHDPS. The collection of high-resolution synchrotron X-ray data has been reported recently [43]. Crystals were pseudo-merohedrally twinned to give the illusion of tetragonal symmetry, with a twin fraction of 0.46

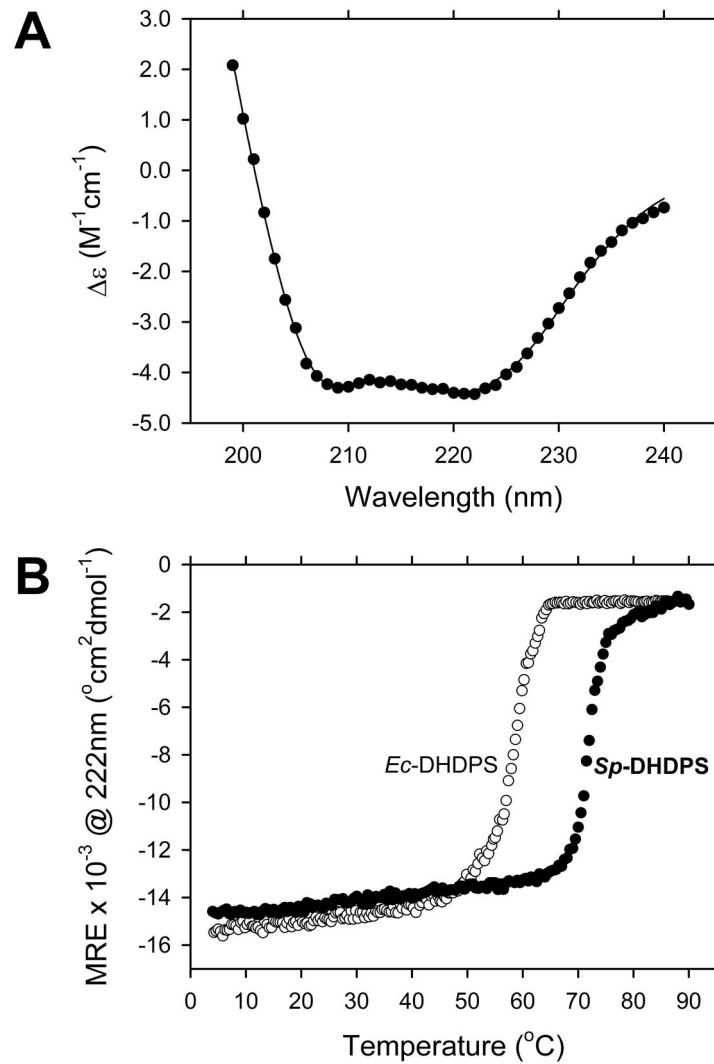


Figure 3. Circular dichroism spectroscopy of *Sp*-DHDPS. (A) CD spectrum of *Sp*-DHDPS (●) plotted as the molar circular dichroism ($\Delta\epsilon$) as a function of wavelength. The solid line represents the nonlinear least squares fit using the CONTINLL algorithm and SP43 database within the CDPRO software suite [48,49]. The best-fit resulted in the secondary structure composition reported in Table 3. (B) Thermal denaturation profiles of *Sp*-DHDPS (●) and *Ec*-DHDPS (○) plotted as mean residue ellipticity (MRE) versus temperature. The apparent melting temperature (T_M^{app}), or midpoint of the transition between folded and unfolded states, was determined from the ordinate maximum of a plot of the first derivative of the MRE as a function of temperature to yield 59°C for *Ec*-DHDPS and 72°C for *Sp*-DHDPS.

doi: 10.1371/journal.pone.0083419.g003

(Table 2). Moreover, the apparent 4_2 screw axis was characterized by significant systematic absence violations, which led after abortive attempts in $P4_22_12$ to solution and refinement in the monoclinic space group $P2_1$ where there is ambiguity with respect to the twin law. However, with two well-defined 2_1 screw axes perpendicular to the pseudo-tetragonal axis, final refinements proceeded successfully in the orthorhombic space group $P22_12_1$ with the twinning axis being parallel to the pseudo-tetrad. Only in this final assignment of crystallographic symmetry did the C-terminal residues 302-311 (see below) become well defined. The structure has been refined at 1.9 Å resolution (Table 2) to an R_{work} of 16.5 % (R_{free}

Table 3. Secondary structure composition of *Sp*-DHDPS and *Ec*-DHDPS determined by CD spectroscopy[†].

Enzyme	α -helix	β -strand	turn	unordered	RMSD
<i>Sp</i> -DHDPS	36	15	20	29	0.05
<i>Ec</i> -DHDPS	34	17	20	29	0.04

[†] Parameters resulting from the nonlinear best-fit using the CONTINLL algorithm and SP43 database within the CDPRO software suite [48,49].

doi: 10.1371/journal.pone.0083419.t003

Table 4. Comparison of the thermostability and hydrodynamic properties of *Sp*-DHDPS and *Ec*-DHDPS derived from circular dichroism spectroscopy and analytical ultracentrifugation studies.

Enzyme	$T_M^{\text{app}1}$ °C	$s_{20,w}$ (S)	M_r^4 (kDa)	M (kDa)	ff_0^6	a/b^7	K_D^{42} (nM)
<i>Sp</i> -DHDPS	72	7.2 ²	135	133 ⁵	1.25 ⁶	2.2	1.7 ⁸
<i>Ec</i> -DHDPS	59	6.9 ³	125	128 ³	1.26 ³	2.6	76 ³

¹ The apparent melting temperature (T_M^{app}), or midpoint of the transition between folded and unfolded states, was determined from the ordinate maximum of a plot of the first derivative of the MRE as a function of temperature.

² Value determined experimentally from the ordinate maximum of the $c(s)$ distribution best-fit shown in Figure 4A.

³ Hydrodynamic properties reported in [34].

⁴ Molecular mass calculated from the amino acid sequence.

⁵ Value calculated experimentally from the apparent molecular mass taken from the ordinate maximum of the $c(M)$ distribution best-fit shown in Figure 4B.

⁶ Frictional ratio calculated using the partial specific volume (v) method employing SEDNTERP software [53,54].

⁷ Axial-ratio as calculated from the program SEDNTERP using the method assuming a prolate ellipsoid.

⁸ The tetramer-dimer dissociation constant calculated from the global nonlinear least squares best-fit described in Figure 5

doi: 10.1371/journal.pone.0083419.t004

of 21.2 %). Two residues, V147 and Y114 in both chains A and B lie in disallowed Ramachandran conformers, but are clearly defined in the electron density. Both residues are located at the 'tight' dimer interface (Figure 7) and are held in strained conformations by hydrogen bonding and hydrophobic packing at this interface. The strained conformation of the highly conserved Y114 (Figure 1B) has been observed in all DHDPS structures determined to date, including those from plants [20-36]. However, the strained conformation of V147, which is poorly conserved (Figure 1B), appears to be unique to *Sp*-DHDPS.

Consistent with the solution studies, *Sp*-DHDPS forms a homotetrameric structure (PDB ID: 3VFL) that is depicted in Figure 7. Each monomer unit is folded to form an N-terminal (β/α)₈-barrel (residues 2-229) with a C-terminal extension comprised of three helices (residues 232-292). The C-terminal residues 302-311 lie in a groove formed by the 'tight' dimer interface (i.e. the interface between chains A & B or C & D in Figure 7). As with other DHDPS structures, including *E. coli* DHDPS [25,31], the active site of *Sp*-DHDPS is located within the β -barrel of each subunit. Many of the residues adopt a similar spatial arrangement to that of the *Ec*-DHDPS structure [PDB ID: 1YXC] [25] (Figure 8A). The key lysine residue, K168, which forms a Schiff base with the pyruvate substrate, is present alongside residues Y140, R145, and G192, which play a pivotal role in the cyclization after reaction with the second substrate (S)-ASA [25,70] (Figure 8A). Two of the residues forming the catalytic triad, which serves to shuttle protons to and from the active site (i.e. Y140 and T50), are also present in a similar orientation to the equivalent residues from the *E. coli* ortholog (Figure 8A). However, the third residue of the catalytic triad, Y114, undergoes a $\sim 70^\circ$ rotation in the active site of *Sp*-

DHDPS relative to the equivalent residue of the *E. coli* enzyme (i.e. Y107), although the functionally important -OH group is similarly positioned. This residue interdigitates across the 'tight' dimer interface forming a hydrophobic stack with Y113 from the adjacent monomer (Figure 8B). This 70° rotation serves to change the interaction to a π stacking between the two tyrosine residues.

Relative to the *Ec*-DHDPS structure (PDB ID: 1YXC) [26], insight into the enhanced stability observed for *Sp*-DHDPS in solution is revealed by close inspection of the interactions stabilizing the 'tight' dimer interface, and in particular, the 'weak' dimer interface (Figure 7, interface AC or BD). Analysis of the solvent inaccessible surface areas (SISA), calculated using the Protein Interfaces, Surfaces and Assemblies (PISA) program [71], reveals that the 'tight' dimer interface of *Sp*-DHDPS (Figure 7, interface AB or CD) buries 1350 Å² (Table 6, Figure 9A), slightly more than that calculated (1290 Å²) for the equivalent interface of the *Ec*-DHDPS structure (Table 6, Figure 9C). Although both enzymes contain the same number of residues (i.e. 38 in total) at this interface, *Sp*-DHDPS contains a larger proportion of residues forming hydrogen bonds. In contrast, the 'weak' dimer interface has a total SISA of 800 Å² (Table 6, Figure 9B), which is significantly greater than the equivalent interface of the *E. coli* structure (500 Å²) (Table 6 & Figure 9D). The substantially larger buried surface area in *Sp*-DHDPS is due to a greater number of residues forming contacts at this interface. In addition, it is interesting to note that this enzyme also contains three residues that form salt bridge interactions, a feature that is absent in *Ec*-DHDPS (Table 6 & Figure 9D).

Discussion

Streptococcus pneumoniae is one of the leading causes of disease in the world. In the United States, for example, the organism is responsible for 500,000 cases of pneumonia, 50,000 cases of bacteremia, and 3,000 cases of meningitis per annum [3,72]. Current treatment relies primarily upon the use of penicillin-based antibiotics. However, this approach has had significant limitations given the emergence of drug-resistant *S. pneumoniae* (DRSP). The appearance of multiple drug resistant (MDR) strains in recent times and the occurrence of community acquired infection are also of particular concern [72,73]. Accordingly, there is an urgent need to develop novel antimicrobials and an equally urgent need to discover new antibiotic targets. A promising pneumococcal drug target is DHDPS, given the enzymes function in producing lysine required for protein and cell wall synthesis. However, our knock-out studies show that the $\Delta dapA$ strain of *S. pneumoniae* is a lysine auxotroph (Figure 2), which suggests DHDPS attenuated strains may be able to survive *in vivo* by scavenging exogenous lysine from the host. Further studies are required to ascertain the viability of the $\Delta dapA$ strain *in vivo*. Nevertheless, having established the $\Delta dapA$ strain was essential to *S. pneumoniae* in minimal media, we set out to characterize the structure, function and stability of the enzyme to afford insight into rational drug design strategies to afford the discovery of *Sp*-DHDPS inhibitors in future work.

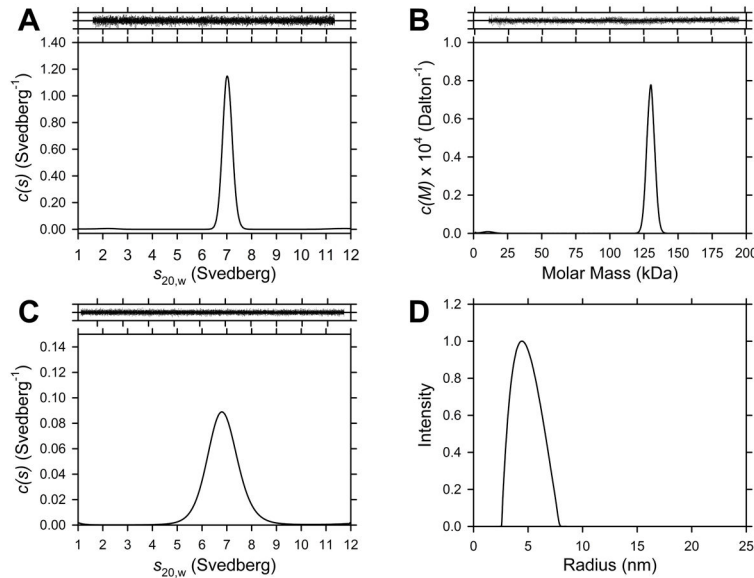


Figure 4. Sedimentation velocity and dynamic light scattering analyses of *Sp*-DHDPS. (A) Continuous sedimentation coefficient, $c(s)$, distribution of *Sp*-DHDPS at 4.5 μM plotted as a function of standardized sedimentation coefficient ($s_{20,w}$) with RMSD and runs test Z values for the best-fit of 0.008 and 6.6, respectively. (B) Continuous mass, $c(M)$, distribution of *Sp*-DHDPS at a concentration of 4.5 μM plotted as a function of molar mass with RMSD and runs test Z values of 0.008 and 6.6 respectively. (C) $c(s)$ distribution of *Sp*-DHDPS at 740 nM, with RMSD and runs test Z values of 0.02 and 1.64, respectively. Data were analyzed employing the program SEDFIT [51,52,65,66] using a resolution (N) of 200 and a sedimentation coefficient range of 0.1-12 S or molar mass range 1.0-250 kDa with a P-value of 0.95. Above Panels A-C: Residuals plotted as a function of radial position resulting from continuous size-distribution best-fits shown in panels A-C. (D) A distribution plot of the average unweighted hydrodynamic radii of *Sp*-DHDPS at a concentration of 59 μM determined using dynamic light scattering (DLS). The results of the distribution plot reveal an average hydrodynamic radius of 4.5 ± 0.2 nm.

doi: 10.1371/journal.pone.0083419.g004

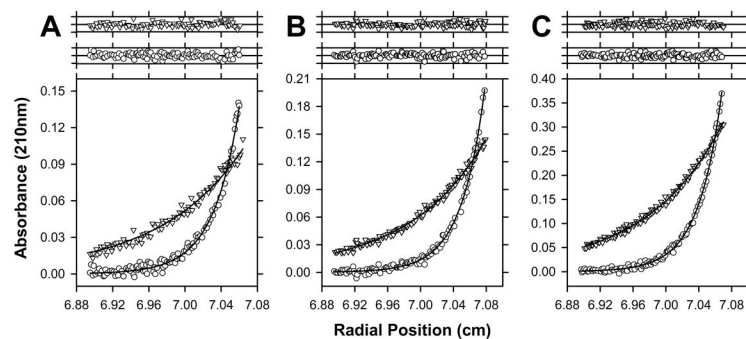


Figure 5. Sedimentation equilibrium analyses of *Sp*-DHDPS. Absorbance at sedimentation equilibrium is plotted as a function of radial position for *Sp*-DHDPS at an initial concentration of (A) 296 nM; (B) 355 nM and (C) 740 nM. Data was measured at 210 nm and rotor speeds of 10,000 rpm (\circ) and 18,000 rpm (\triangle). The resulting global nonlinear least squares fit to a dimer-tetramer equilibrium model is shown as solid lines and yielded a K_D^{4a2} of 1.7 nM with a global reduced χ^2 of 0.5. Above Panels A-C: Residuals plotted as a function of radial position resulting from the global nonlinear best-fit analysis to a dimer-tetramer model for data at 10,000 rpm (\circ) and 18,000 rpm (\triangle).

doi: 10.1371/journal.pone.0083419.g005

Our studies show that *Sp*-DHDPS is similar in some respects to the well characterized ortholog from *E. coli*, which shares 36 % sequence identity. For instance, CD spectroscopy and AUC studies reveals that *Sp*-DHDPS, like *Ec*-DHDPS, has high α/β

secondary structure (Table 3, Figure 3A) and resides in a dimer-tetramer equilibrium (Table 4, Figures 4 and 5). Likewise, enzyme kinetic studies demonstrate both *Sp*-DHDPS and *Ec*-DHDPS operate via a Ping-Pong catalytic mechanism.

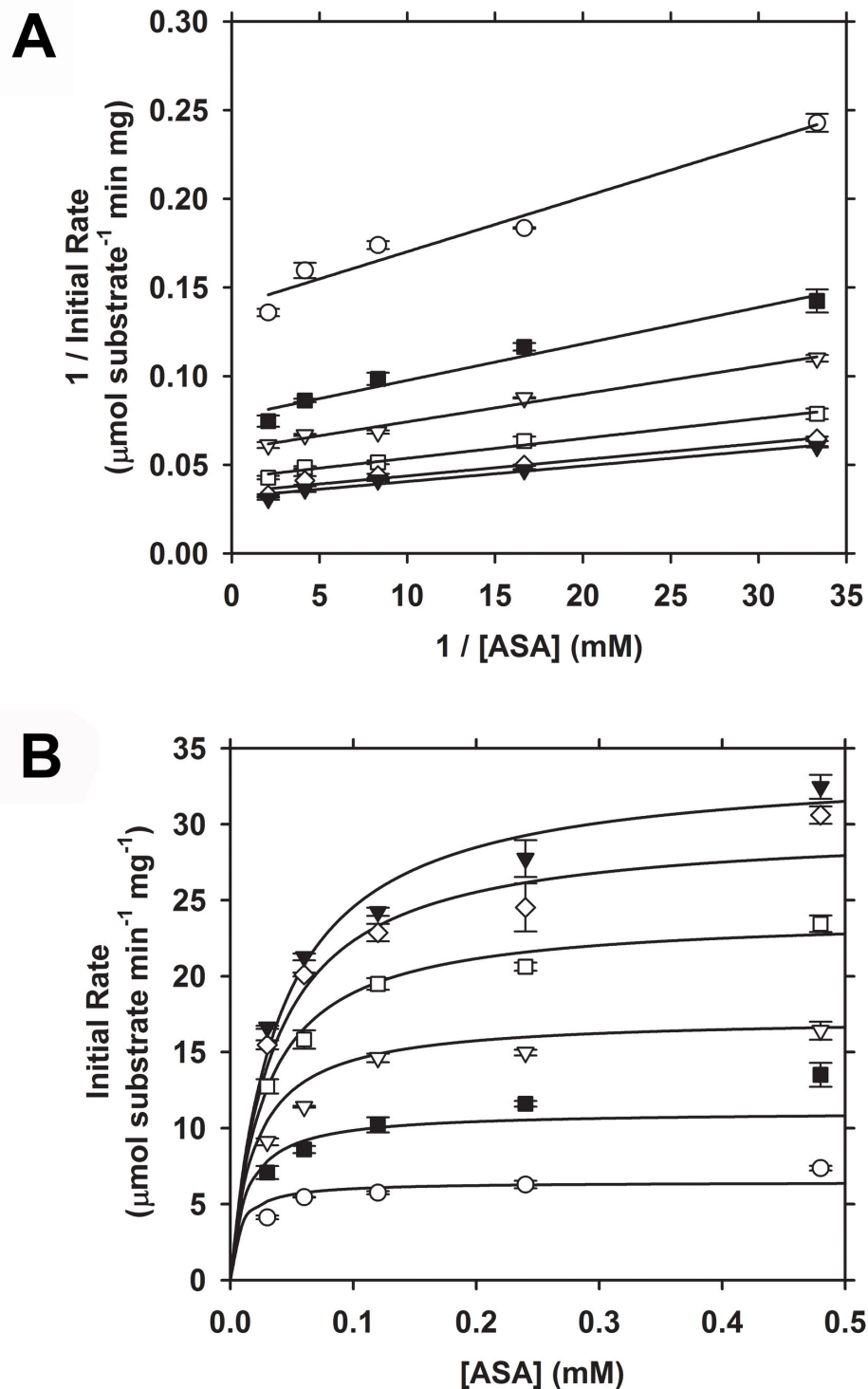


Figure 6. Enzyme kinetic profiles of recombinant *Sp*-DHDPS. Initial velocity was measured as a function of (*S*)-ASA concentration. Experiments were conducted at fixed pyruvate concentrations of (○) 0.5 mM, (◊) 1.0 mM, (◻) 2.0 mM, (◻) 4.0 mM, (◻) 8.0 mM and (◻) 16.0 mM. (A) Lineweaver-Burk plots showing multiple parallel lines; diagnostic of a ping pong kinetic mechanism [25,67,69]. (B) Michaelis-Menten plots of data shown in A, where solid lines represent the global nonlinear best-fit to a Ping-Pong mechanism (without substrate inhibition) using ENZFITTER software, resulting in a $R^2 = 0.98$ and the enzyme kinetic parameters summarized in Table 5.

doi: 10.1371/journal.pone.0083419.g006

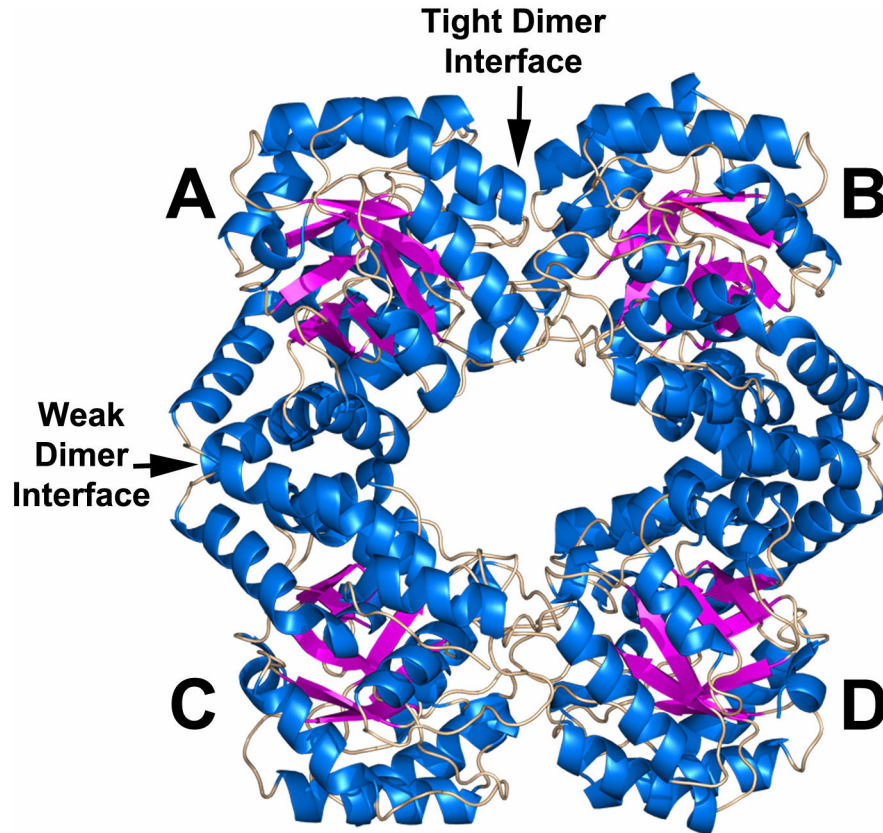


Figure 7. Crystal structure of *Sp*-DHDPS determined at a resolution of 1.9 Å. The enzyme crystallizes as a tetramer comprised of four identical subunits labeled A, B, C & D with subunits AB or CD connected *via* the 'tight' dimer interface, and subunits AC or BD connected *via* the 'weak' dimer interface.

doi: 10.1371/journal.pone.0083419.g007

Table 5. Summary of the enzyme kinetic parameters of *Sp*-DHDPS compared to *Ec*-DHDPS.

Enzyme	k_{cat} (sec ⁻¹)	K_M^{ASA} (mM)	K_M^{PYR} (mM)
<i>Sp</i> -DHDPS	22	0.044 ± 0.003	2.55 ± 0.05
<i>Ec</i> -DHDPS [†]	124	0.11 ± 0.01	0.26 ± 0.03

[†] Kinetic parameters reported in [25].

doi: 10.1371/journal.pone.0083419.t005

However, the enzyme kinetic parameters calculated for *Sp*-DHDPS are significantly different to the *E. coli* enzyme (Table 5). The greater K_M^{PYR} for *Sp*-DHDPS suggests a lower thermodynamic affinity for this substrate (assuming the coupling of pyruvate with (S)-ASA is rate-determining), consistent with the very strongly associated, and presumably more rigid tetramer, that hinders access of pyruvate to the binding site and relaxation of the protein to accommodate pyruvate. This is consistent with our prior conclusions that protein dynamics control enzyme kinetics [26,27,36,74].

It is worthwhile noting that pyruvate is a central metabolite, serving as a substrate for several other enzymes. Pyruvate-

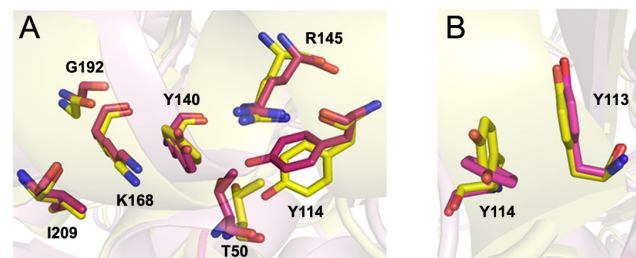


Figure 8. Comparison of the active sites of *Sp*-DHDPS (yellow) and *Ec*-DHDPS (pink). (A) An overlay of the active site with residues labeled according to *Sp*-numbering. (B) Image demonstrating the approximate 70° rotation of Y114 in the active site of *Sp*-DHDPS compared to the equivalent residue in *Ec*-DHDPS (Y107).

doi: 10.1371/journal.pone.0083419.g008

utilizing enzymes, such as pyruvate dehydrogenase and lactate dehydrogenase from Gram-positive bacterial species, including *Bacillus subtilis*, *Corynebacterium glutamicum* and *Lactococcus lactis*, display K_M^{PYR} ranging 1 - 15 mM [75,76]. These values are considerably higher than orthologs from

Table 6. Comparison of the 'tight' dimer and 'weak' dimer interfaces of Sp-DHDPS and Ec-DHDPS.

Enzyme	Tight Dimer SISA [†] (Å ²)		Residues involved in Hydrogen bonding		Residues involved in Ion interactions		Weak Dimer SISA [†] (Å ²)		Residues involved in Hydrophobic contacts		Residues involved in Hydrogen bonding		Residues involved in Ion interactions	
	1350	1290	11	7	0	0	800	500	20	11	4	6	3	0
Sp-DHDPS	27	31												
Ec-DHDPS														

[†] SISA = solvent inaccessible surface area. Calculated employing PISA [71] analysis (http://www.ebi.ac.uk/msd-srv/prot_intlistart) and PDB coordinates for Sp-DHDPS (PDB ID: 3VFL) and Ec-DHDPS (PDB ID: 1YXC).
doi: 10.1371/journal.pone.0083419.t006

Gram-negative species, such as *E. coli* and *Thermotoga maritima*, where K_M^{PYR} values range from 0.018 - 0.43 mM [77-79]. These differences, found also in comparison of DHDPS from Gram-positive and Gram-negative species, may indicate that pyruvate is present at a higher intracellular steady-state concentration in *S. pneumoniae* (and other Gram-positive bacteria) than in *E. coli* (and other Gram-negative bacteria). The origins of these differences in K_M^{PYR} are not apparent from the structures of these DHDPS enzymes.

Solution studies also showed Sp-DHDPS possesses significantly greater thermostability compared to Ec-DHDPS (Figure 3B). We subsequently demonstrated using analytical ultracentrifugation that the enhanced thermostability of Sp-DHDPS is contributed by a 45-fold tighter tetramer-dimer dissociation constant (Table 4) [34]. We therefore determined the three-dimensional structure of Sp-DHDPS using X-ray crystallography (Figure 7) to provide insight into the enhanced thermal and thermodynamic stability. The origin of the enhanced thermal stability is clearly revealed in the 1.9 Å resolution crystal structure of Sp-DHDPS (Figure 7) that shows a tetrameric structure of the enzyme, consistent with our solution studies (Table 4, Figures 4 and 5). The tertiary and quaternary structure architecture of Sp-DHDPS is very similar to Ec-DHDPS [25,31,34] with an overall RMSD for superposition of the tetramers of 1.1 Å (alpha carbon atoms), as well as to other structurally characterized bacterial DHDPS enzymes [16-19,22,24-27,29-36]. However, significant structural differences are observed between Sp-DHDPS and Ec-DHDPS at the subunit interfaces (Figure 9). We show that there is an increase of 60 Å² and 300 Å² in solvent-inaccessible surface area (SISA) at the 'tight' dimer and 'weak' dimer interfaces of Sp-DHDPS, respectively (Table 6, Figure 9). This significant increase in SISA, in combination with the greater proportion of hydrogen bonding residues at the 'tight' dimer interface, as well as the presence of residues participating in salt bridge interactions at the 'weak' dimer interface (also referred to as the tetramerization interface [36]), is consistent with the 45-fold lower tetramer-dimer dissociation constant for Sp-DHDPS (Table 4, Figure 5), and to its considerably higher thermal stability (Figure 3B). Consistent with previous studies of other DHDPS enzymes, the residues that form interactions at the 'weak' dimer interface are poorly conserved in Sp-DHDPS, whereas strong conservation is observed at the 'tight' dimer interface where the active sites are located [16-36]. Given that recent studies show dimeric mutants of DHDPS have significantly attenuated catalytic function compared to the wild-type tetramers [26,27,36], the poor conservation at the 'weak' dimer interface offers potential for the design of pathogen-specific antimicrobial agents [34], particularly given that protein-protein interfaces represent highly specific drug targets [80,81]. Indeed, with the increase in drug-resistant bacteria linked to the overuse and misuse of broad spectrum antibiotics [8,9], exploiting the 'weak' dimer interface of Sp-DHDPS may provide a means to negate the incidence of broad spectrum drug resistance.

In conclusion, through gene knock-out studies, circular dichroism spectroscopy, analytical ultracentrifugation, dynamic light scattering, enzyme kinetics and X-ray crystallography

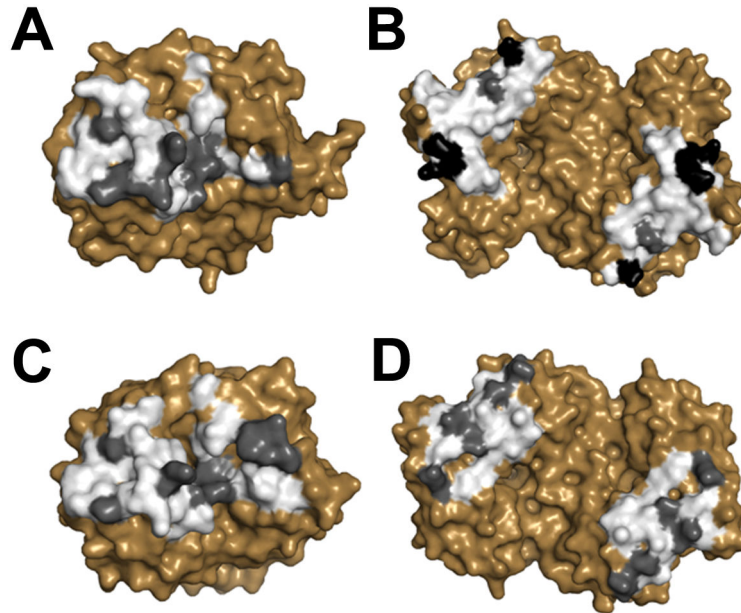


Figure 9. Comparison of the oligomeric interfaces of DHDPS from *S. pneumoniae* (panels A & B) and *E. coli* (panels C & D). Noncovalent interactions and solvent-inaccessible surface area (SISA) were calculated using the program PISA [71]. The ‘tight’ dimer interface of *Sp*-DHDPS (panel A) buries 1350 Å² of SISA compared to *Ec*-DHDPS (panel C), which buries 1290 Å² of SISA. The ‘weak’ dimer interface of *Sp*-DHDPS (panel B) buries 800 Å² of SISA compared to 500 Å² for *Ec*-DHDPS (panel D). White, grey and black shaded regions correspond to interfacing, hydrogen bonding and ion bonding residues, respectively.

doi: 10.1371/journal.pone.0083419.g009

studies, we demonstrate that *Sp*-DHDPS is an essential, active and thermostable tetramer. Our work offers insight into rational drug design strategies targeting multiple sites of the enzyme to afford the discovery of novel antibiotic agents with potential to negate drug resistance.

Acknowledgements

We acknowledge Geoff Hogg (Microbiological Diagnostic Unit, University of Melbourne) for providing genomic DNA, the friendly staff of the Bio21-C³, the MX beamline scientists at the Australian Synchrotron, Suresh. K. Bhargava (School of Applied Sciences, RMIT University) for access to dynamic light

scattering equipment and Craig A. Hutton (School of Chemistry, University of Melbourne) and Renwick C.J. Dobson (School of Biological Sciences, University of Canterbury) for useful discussion during preparation of this manuscript.

Author Contributions

Conceived and designed the experiments: MAP MWP RMRB. Performed the experiments: CD GB JP LMZ MAG NEK. Analyzed the data: CD GB GBJ HDM JP JY LMZ MAG MAP NEK. Contributed reagents/materials/analysis tools: FGP JAG JY MDWG. Wrote the manuscript: CD GBJ JP MAG MAP LMZ.

References

- Moscoso M, García E, López R (2006) Biofilm formation by *Streptococcus pneumoniae*: role of choline, extracellular DNA, and capsular polysaccharide in microbial accretion. *J Bacteriol* 188: 7785-7795. doi:10.1128/JB.00673-06. PubMed: 16936041.
- Janssens JP, Krause KH (2004) Pneumonia in the very old. *Lancet Infect Dis* 4: 112-124. doi:10.1016/S1473-3099(04)00931-4. PubMed: 14871636.
- Cartwright K (2002) Pneumococcal disease in western Europe: burden of disease, antibiotic resistance and management. *Eur J Pediatr* 161: 188-195. doi:10.1007/s00431-001-0907-3. PubMed: 12014384.
- Whitney CG, Farley MM, Hadler J, Harrison LH, Bennett NM et al. (2000) Increasing prevalence of multidrug-resistant *Streptococcus pneumoniae* in the United States. *N Engl J Med* 343: 1917-1924. doi: 10.1056/NEJM200012283432603. PubMed: 11136262.
- Nunes S, Sá-Leão R, Carriço J, Alves CR, Mato R et al. (2005) Trends in drug resistance, serotypes, and molecular types of *Streptococcus pneumoniae* colonizing preschool-age children attending day care centers in Lisbon, Portugal: a summary of 4 years of annual surveillance. *J Clin Microbiol* 43: 1285-1293. doi:10.1128/JCM.43.3.1285-1293.2005. PubMed: 15750097.
- Schrag SJ, McGee L, Whitney CG, Beall B, Craig AS et al. (2004) Emergence of *Streptococcus pneumoniae* with very-high-level resistance to penicillin. *Antimicrob Agents Chemother* 48: 3016-3023. doi:10.1128/AAC.48.8.3016-3023.2004. PubMed: 15273115.
- Stephens DS, Zughaier SM, Whitney CG, Baughman WS, Barker L et al. (2005) Incidence of macrolide resistance in *Streptococcus pneumoniae* after introduction of the pneumococcal conjugate vaccine: population-based assessment. *Lancet* 365: 855-863. doi:10.1016/S0140-6736(05)71043-6. PubMed: 15752529.
- Sørum H, L'Abée-Lund TM (2002) Antibiotic resistance in food-related bacteria—a result of interfering with the global web of bacterial genetics. *Int J Food Microbiol* 78: 43-56. doi:10.1016/S0168-1605(02)00241-6. PubMed: 12222637.
- Wegener HC (2003) Antibiotics in animal feed and their role in resistance development. *Curr Opin Microbiol* 6: 439-445. doi:10.1016/j.mib.2003.09.009. PubMed: 14572534.

10. Kyaw MH, Lynfield R, Schaffner W, Craig AS, Hadler J et al. (2006) Effect of introduction of the pneumococcal conjugate vaccine on drug-resistant *Streptococcus pneumoniae*. N Engl J Med 354: 1455-1463. doi:10.1056/NEJMoa051642. PubMed: 16598044.
11. Dogovski C, Atkinson SC, Dommaraju SR, Hor L, Dobson RCJ, et al. (2009) Lysine biosynthesis in bacteria – an uncharted pathway for novel antibiotic design. In: H Doelle. Encyclopedia of life support systems, Volume 11 (Biotechnology Part I). Oxford: EOLSS Publishers. pp 116–136
12. Dogovski C, Atkinson SC, Dommaraju SR, Downton M, Hor L et al. (2012) Enzymology of bacterial lysine biosynthesis. In: D Ekinici. Biochemistry: InTech Open Access Publisher. pp 225-262.
13. Hutton CA, Perugini MA, Gerrard JA (2007) Inhibition of lysine biosynthesis: an emerging antibiotic strategy. Mol Biosyst 3: 458-465. doi:10.1039/b705624a. PubMed: 17579770.
14. Yugari Y, Gilvarg C (1965) The condensation step in diaminopimelate synthesis. J Biol Chem 240: 4710-4716. PubMed: 5321309.
15. Hutton CA, Southwood TJ, Turner JJ (2003) Inhibitors of lysine biosynthesis as antibacterial agents. Mini Rev Med Chem 3: 115-127. doi:10.2174/1389557033405359. PubMed: 12570844.
16. Burgess BR, Dobson RCJ, Bailey MF, Atkinson SC, Griffin MDW et al. (2008) Structure and evolution of a novel dimeric enzyme from a clinically-important bacterial pathogen. J Biol Chem 283: 27598-27603. doi:10.1074/jbc.M804231200. PubMed: 18684709.
17. Girish TS, Sharma E, Gopal B (2008) Structural and functional characterization of *Staphylococcus aureus* dihydrodipicolinate synthase. FEBS Lett 582: 2923-2930. doi:10.1016/j.febslet.2008.07.035. PubMed: 18671976.
18. Kaur N, Gautam A, Kumar S, Singh A, Singh N et al. (2011) Biochemical studies and crystal structure determination of dihydrodipicolinate synthase from *Pseudomonas aeruginosa*. Int J Biol Macromol 48: 779-787. doi:10.1016/j.ijbiomac.2011.03.002. PubMed: 21396954.
19. Schnell R, Oehlmann W, Sandalova T, Braun Y, Huck C et al. (2012) Tetrahydrodipicolinate N-succinyltransferase and dihydrodipicolinate synthase from *Pseudomonas aeruginosa*: structure analysis and gene deletion. PLOS ONE 7: e31133. doi:10.1371/journal.pone.0031133. PubMed: 22359568.
20. Atkinson SC, Dogovski C, Downton MT, Pearce FG, Reboul CF et al. (2012) Crystal, solution and *in silico* structural studies of dihydrodipicolinate synthase from the common grapevine. PLOS ONE 7: e38318. doi:10.1371/journal.pone.0038318. PubMed: 22761676.
21. Atkinson SC, Dogovski C, Downton MT, Czabotar PE, Dobson RCJ et al. (2013) Structural, kinetic and computational investigation of *Vitis vinifera* DHDPS reveals new insight into the mechanism of lysine-mediated allosteric inhibition. Plant Mol Biol 81: 431-446. doi:10.1007/s11103-013-0014-7. PubMed: 23354837.
22. Blagova E, Levdivikov V, Miloti N, Fogg MJ, Kalliomaa AK et al. (2006) Crystal structure of dihydrodipicolinate synthase (BA3935) from *Bacillus anthracis* at 1.94 Å resolution. Proteins 62: 297-301. PubMed: 16287120.
23. Blickling S, Beisel HG, Bozic D, Knäblein J, Laber B et al. (1997) Structure of dihydrodipicolinate synthase of *Nicotiana glauca* reveals novel quaternary structure. J Mol Biol 274: 608-621. doi:10.1006/jmbi.1997.1393. PubMed: 9417939.
24. Devenish SRA, Huisman FHA, Parker EJ, Hadfield AT, Gerrard JA (2009) Cloning and characterisation of dihydrodipicolinate synthase from the pathogen *Neisseria meningitidis*. Biochim Biophys Acta 1794: 1168-1174. doi:10.1016/j.bbapap.2009.02.003. PubMed: 19236959.
25. Dobson RC, Griffin MD, Jameson GB, Gerrard JA (2005) The crystal structures of native and (S)-lysine-bound dihydrodipicolinate synthase from *Escherichia coli* with improved resolution show new features of biological significance. Acta Crystallogr D Biol Crystallogr 61: 1116-1124. doi:10.1107/S0907444905016318. PubMed: 16041077.
26. Griffin MDW, Dobson RCJ, Pearce FG, Antonio L, Whitten AE et al. (2008) Evolution of quaternary structure in a homotetrameric protein. J Mol Biol 380: 691-703. doi:10.1016/j.jmb.2008.05.038. PubMed: 18556019.
27. Griffin MDW, Dobson RCJ, Gerrard JA, Perugini MA (2010) Exploring the dimer-dimer interface of the dihydrodipicolinate synthase tetramer: how resilient is the interface? Arch Biochem Biophys 494: 58-63. doi: 10.1016/j.abb.2009.11.014. PubMed: 19919824.
28. Griffin MDW, Billakanti JM, Wason A, Keller S, Mertens HDT et al. (2012) Characterisation of lysine biosynthetic enzymes in *Arabidopsis thaliana*. PLOS ONE 7: e40318. doi:10.1371/journal.pone.0040318. PubMed: 22792278.
29. Kang BS, Kim YG, Ahn JW, Kim KJ (2010) Crystal structure of dihydrodipicolinate synthase from *Hahella chejuensis* at 1.5 Å resolution. Int J Biol Macromol 46: 512-516. doi:10.1016/j.ijbiomac.2010.03.005. PubMed: 20227435.
30. Kefala G, Evans GL, Griffin MD, Devenish SR, Pearce FG et al. (2008) Crystal structure and kinetic study of dihydrodipicolinate synthase from *Mycobacterium tuberculosis*. Biochem J 411: 351-360. doi:10.1042/BJ20071360. PubMed: 18062777.
31. Mirwaldt C, Korndörfer I, Huber R (1995) The crystal structure of dihydrodipicolinate synthase from *Escherichia coli* at 2.5 Å resolution. J Mol Biol 246: 227-239. doi:10.1006/jmbi.1994.0078. PubMed: 7853400.
32. Padmanabhan B, Strange RW, Antonyuk SV, Ellis MJ, Hasnain SS et al. (2009) Structure of dihydrodipicolinate synthase from *Methanocaldococcus jannaschii*. Acta Crystallogr Sect F Struct Biol Cryst Commun 65: 1222-1226. doi:10.1107/S0907444909037421. PubMed: 20054116.
33. Pearce FG, Perugini MA, Mc Kerchar HJ, Gerrard JA (2006) Dihydrodipicolinate synthase from *Thermotoga maritima*. Biochem J 400: 359-366. doi:10.1042/BJ20060771. PubMed: 16872276.
34. Perugini MA, Griffin MDW, Smith BJ, Webb LE, Davis AJ et al. (2005) Insight into the self-association of key enzymes from pathogenic species. Eur Biophys J 34: 469-476. doi:10.1007/s00249-005-0491-y. PubMed: 15981001.
35. Rice EA, Bannon GA, Glenn KC, Jeong SS, Sturman EJ et al. (2008) Characterization and crystal structure of lysine insensitive *Corynebacterium glutamicum* dihydrodipicolinate synthase (cDHDPS) protein. Arch Biochem Biophys 480: 111-121. doi:10.1016/j.abb.2008.09.018. PubMed: 18930704.
36. Voss JE, Scally SW, Taylor NL, Atkinson SC, Griffin MDW et al. (2010) Substrate-mediated stabilization of a tetrameric drug target reveals achilles heel in anthrax. J Biol Chem 285: 5188-5195. doi:10.1074/jbc.M109.038166. PubMed: 19948665.
37. Wei BP, Shepherd RK, Robins-Browne RM, Clark GM, O'Leary SJ (2006) Pneumococcal meningitis: development of a new animal model. Otol Neurotol 27: 844-854. doi:10.1097/01.mao.0000231603.25961.f1. PubMed: 16936571.
38. Van de Rijn I, Kessler RE (1980) Growth characteristics of group A streptococci in a new chemically defined medium. Infect Immun 27: 444-448. PubMed: 6991416.
39. Sambrook J, Fritsch EF, Maniatis T (1989) Molecular cloning: A Laboratory Manual. Cold Spring Harbor: Cold Spring Harbor Laboratory Press.
40. Chalker AF, Minehart HW, Hughes NJ, Koretke KK, Lonetto MA et al. (2001) Systematic identification of selective essential genes in *Helicobacter pylori* by genome prioritization and allelic replacement mutagenesis. J Bacteriol 183: 1259-1268. doi:10.1128/JB.183.4.1259-1268.2001. PubMed: 11157938.
41. Macrina FL, Tobian JA, Jones KR, Evans RP, Clewell DB (1982) A cloning vector able to replicate in *Escherichia coli* and *Streptococcus sanguis*. Gene 19: 345-353. doi:10.1016/0378-1119(82)90025-7. PubMed: 6295886.
42. Pozzi G, Masala L, Iannelli F, Manganelli R, Høy Varstein LS et al. (1996) Competence for genetic transformation in encapsulated strains of *Streptococcus pneumoniae*: two allelic variants of the peptide pheromone. J Bacteriol 178: 6087-6090. PubMed: 8830714.
43. Sibarani NE, Gorman MA, Dogovski C, Parker MW, Perugini MA (2010) Crystallization of dihydrodipicolinate synthase from a clinical isolate of *Streptococcus pneumoniae*. Acta Crystallogr Sect F Struct Biol Cryst Commun 66: 32-36. doi:10.1107/S0108767309041749. PubMed: 20057065.
44. Domigan LJ, Scally SW, Fogg MJ, Hutton CA, Perugini MA et al. (2009) Characterisation of dihydrodipicolinate synthase from *Bacillus anthracis*. Biochim Biophys Acta 1794: 1510-1516. doi:10.1016/j.bbapap.2009.06.020. PubMed: 19595801.
45. Karsten WE (1997) Dihydrodipicolinate synthase from *Escherichia coli*: pH dependent changes in the kinetic mechanism and kinetic mechanism of allosteric inhibition by L-lysine. Biochemistry 36: 1730-1739. doi:10.1021/bi962264x. PubMed: 9048556.
46. Roberts SJ, Morris JC, Dobson RCJ, Gerrard JA (2003) The preparation of (S)-aspartate semi-aldehyde appropriate for use in biochemical studies. Bioorg Med Chem Lett 13: 265-267. PubMed: 12482436.
47. Davis AJ, Perugini MA, Smith BJ, Stewart JD, Ilg T et al. (2004) Properties of GDP-mannose pyrophosphorylase, a critical enzyme and drug target in *Leishmania mexicana*. J Biol Chem 279: 12462-12468. PubMed: 14718535.
48. Sreerama N, Venyaminov SY, Woody RW (2000) Estimation of protein secondary structure from circular dichroism spectra: inclusion of denatured proteins with native proteins in the analysis. Anal Biochem 287: 243-251. doi:10.1006/abio.2000.4879. PubMed: 11112270.

49. Sreerama N, Woody RW (2000) Estimation of protein secondary structure from circular dichroism spectra: comparison of CONTIN, SELCON, and CDSSTR methods with an expanded reference set. *Anal Biochem* 287: 252-256. doi:10.1006/abio.2000.4880. PubMed: 11112271.
50. McLennan N, Masters M (1998) GroE is vital for cell-wall synthesis. *Nature* 392: 139. doi:10.1038/32317. PubMed: 9515958.
51. Schuck P (2000) Size-distribution analysis of macromolecules by sedimentation velocity ultracentrifugation and Lamm equation modeling. *Biophys J* 78: 1606-1619. doi:10.1016/S0006-3495(00)76713-0. PubMed: 10692345.
52. Schuck P, Perugini MA, Gonzales NR, Howlett GJ, Schubert D (2002) Size-distribution analysis of proteins by analytical ultracentrifugation: strategies and application to model systems. *Biophys J* 82: 1096-1111. doi:10.1016/S0006-3495(02)75469-6. PubMed: 11806949.
53. Hayes DB, Laue T, Philo J (2003) Sedimentation Interpretation Program, Version 1.08. Durham, New Hampshire: University of New Hampshire.
54. Laue TM, Shah BD, Ridgeway TM, Pelletier SL (1992) Computer-aided interpretation of analytical sedimentation data for proteins. In SE HardingAJ, RoweJC, Horton, Analytical ultracentrifugation in biochemistry and polymer science. Royal Society of Chemistry, Cambridge, UK. pp 90-125.
55. Vistica J, Dam J, Balbo A, Yikilmaz E, Mariuzza RA et al. (2004) Sedimentation equilibrium analysis of protein interactions with global implicit mass conservation constraints and systematic noise decomposition. *Anal Biochem* 326: 234-256. doi:10.1016/j.ab.2003.12.014. PubMed: 15003564.
56. McPhillips TM, McPhillips SE, Chiu HJ, Cohen AE, Deacon AM et al. (2002) Blu-Ice and the Distributed Control System: software for data acquisition and instrument control at macromolecular crystallography beamlines. *J Synchrotron Radiat* 9: 401-406. doi:10.1107/S0909049502015170. PubMed: 12409628.
57. Otwinowski Z, Minor W (1997) Processing of X-ray diffraction data collected in oscillation mode. *Methods Enzymol* 276: 307-326. doi:10.1016/S0076-6879(97)76066-X.
58. Evans P (2006) Scaling and assessment of data quality. *Acta Crystallogr D Biol Crystallogr* 62: 72-82. doi:10.1107/S0907444905036693. PubMed: 16369096.
59. McCoy AJ, Grosse-Kunstleve RW, Storoni LC, Read RJ (2005) Likelihood-enhanced fast translation functions. *Acta Crystallogr D Biol Crystallogr* 61: 458-464. doi:10.1107/S0907444905001617. PubMed: 15805601.
60. Adams PD, Grosse-Kunstleve RW, Hung LW, Ioerger TR, McCoy AJ et al. (2002) PHENIX: building new software for automated crystallographic structure determination. *Acta Crystallogr D Biol Crystallogr* 58: 194-1954. PubMed: 12393927.
61. Emsley P, Cowtan K (2004) Coot: model-building tools for molecular graphics. *Acta Crystallogr D Biol Crystallogr* 60: 2126-2132. doi:10.1107/S0907444904019158. PubMed: 15572765.
62. Kabsch W (2010) XDS. *Acta Crystallogr D Biol Crystallogr* 66: 125-132. doi:10.1107/S0907444909047337. PubMed: 20124692.
63. Vagin A (1997) MOLREP: an automated program for molecular replacement. *J Appl Crystallogr* 30: 1022-1025. doi:10.1107/S0021889897006766.
64. Murshudov GN, Vagin AA, Dodson EJ (1997) Refinement of macromolecular structures by the maximum-likelihood method. *Acta Crystallogr D Biol Crystallogr* 53: 240-255. doi:10.1107/S0907444996012255. PubMed: 15299926.
65. Perugini MA, Schuck P, Howlett GJ (2000) Self-association of human apolipoprotein E3 and E4 in the presence and absence of phospholipid. *J Biol Chem* 275: 36758-36765. doi:10.1074/jbc.M005565200. PubMed: 10970893.
66. Perugini MA, Schuck P, Howlett GJ (2002) Differences in the binding capacity of human apolipoprotein E3 and E4 to size-fractionated lipid emulsions. *Eur J Biochem* 269: 5939-5949. doi:10.1046/j.1432-1033.2002.03319.x. PubMed: 12444983.
67. Cornish-Bowden A (2004) Fundamental enzyme kinetics. 3rd edition. Portland Press Ltd, London.
68. Dobson RCJ, Valegård K, Gerrard JA (2004) The crystal structure of three site-directed mutants of *Escherichia coli* dihydrodipicolinate synthase: further evidence for a catalytic triad. *J Mol Biol* 338: 329-339. doi:10.1016/j.jmb.2004.02.060. PubMed: 15066435.
69. Laber B, Gomis-Rüth FX, Romão MJ, Huber R (1992) *Escherichia coli* dihydrodipicolinate synthase. Identification of the active site and crystallization. *Biochem J* 288: 691-695. PubMed: 1463470.
70. Blickling S, Renner C, Laber B, Pohlenz H-D, Holak TA et al. (1997) Reaction mechanism of *Escherichia coli* dihydrodipicolinate synthase investigated by X-ray crystallography and NMR spectroscopy. *Biochemistry* 36: 24-33. doi:10.1021/bi962272d. PubMed: 8993314.
71. Krissinel E, Henrick K (2007) Inference of macromolecular assemblies from crystalline state. *J Mol Biol* 372: 774-797. doi:10.1016/j.jmb.2007.05.022. PubMed: 17681537.
72. Nordberg P, Monnet DL, Cars O (2005) Antibacterial resistance. Background document for the WHO project: priority medicines for Europe and the World. a public health approach to innovation. Geneva: WHO.
73. Novak R, Henriques B, Charpentier E, Normark S, Tuomanen E (1999) Emergence of vancomycin tolerance in *Streptococcus pneumoniae*. *Nature* 399: 590-593. doi:10.1038/21202. PubMed: 10376600.
74. Reboul CF, Porebski BT, Griffin MDW, Dobson RCJ, Perugini MA et al. (2012) Structural and dynamic requirements for optimal activity of the essential bacterial enzyme dihydrodipicolinate synthase. *PLoS Comput Biol* 8: e1002537. PubMed: 22685390.
75. Dietrich C, Nato A, Bost B, Le Maréchal P, Guyonvarch A (2009) Regulation of ldh expression during biotin-limited growth of *Corynebacterium glutamicum*. *Microbiology* 155: 1360-1375. doi:10.1099/mic.0.022004-0. PubMed: 19332837.
76. Garvie EI (1980) Bacterial lactate dehydrogenases. *Microbiol Rev* 44: 106-139. PubMed: 6997721.
77. Dowd SR, Pratt EA, Sun Z-Y, Ho C (1995) Nature and environment of the sulfhydryls of membrane-associated D-lactate dehydrogenase of *Escherichia coli*. *Biochim Biophys Acta* 1252: 278-283. doi:10.1016/0167-4838(95)00121-A. PubMed: 7578234.
78. Ostendorp R, Auerbach G, Jaenicke R (1996) Extremely thermostable L(+)-lactate dehydrogenase from *Thermotoga maritima*: cloning, characterization, and crystallization of the recombinant enzyme in its tetrameric and octameric state. *Protein Sci* 5: 862-873.
79. Sun Z, Do PM, Rhee MS, Govindasamy L, Wang Q et al. (2012) Amino acid substitutions at glutamate-354 in dihydroliipoamide dehydrogenase of *Escherichia coli* lower the sensitivity of pyruvate dehydrogenase to NADH. *Microbiology* 158: 1350-1358. doi:10.1099/mic.0.055590-0. PubMed: 22343352.
80. Gerrard JA, Hutton CA, Perugini MA (2007) Inhibiting protein-protein interactions as an emerging paradigm for drug discovery. *Mini Rev Med Chem* 7: 151-157. doi:10.2174/138955707779802561. PubMed: 17305589.
81. Wells JA, McClendon CL (2007) Reaching for high-hanging fruit in drug discovery at protein-protein interfaces. *Nature* 450: 1001-1009. doi:10.1038/nature06526. PubMed: 18075579.